



PDE-NetGen 1.0: from symbolic PDE representations of physical processes to trainable neural network representations.

Olivier Pannekoucke¹ and Ronan Fablet²

¹INPT-ENM, UMR CNRS CNRM, CERFACS, 42, av. G. Coriolis 31057 Toulouse, France

²IMT-Atlantic, UMR CNRS Lab-STICC, Brest, France

Correspondence: Olivier Pannekoucke (olivier.pannekoucke@meteo.fr)

Abstract. Bridging physics and deep learning is a topical challenge. While deep learning frameworks open avenues in physical science, the design of physically-consistent deep neural network architectures is an open issue. In the spirit of physics-informed NNs, *PDE-NetGen* package provides new means to automatically translate physical equations, given as PDEs, into neural network architectures. *PDE-NetGen* combines symbolic calculus and a neural network generator. The later exploits NN-based implementations of PDE solvers using Keras. With some knowledge of a problem, *PDE-NetGen* is a plug-and-play tool to generate physics-informed NN architectures. They provide computationally-efficient yet compact representations to address a variety of issues, including among others adjoint derivation, model calibration, forecasting, data assimilation as well as uncertainty quantification. As an illustration, the workflow is first presented for the 2D diffusion equation, then applied to the data-driven and physics-informed identification of uncertainty dynamics for the Burgers equation.

1 Introduction

Machine learning and deep learning receive a fast growing interest in geo-science to address open issues, including for instance sub-grid parameterization,

A variety of learning architectures have shown their ability to encode the physics of a problem, especially deep learning schemes which typically involve millions of unknown parameters, while the theoretical reason of this success remains a key issue (Mallat, 2016). A recent research trend has involved the design of lighter neural network (NN) architectures, like ResNets with shared weights (He et al., 2016), while keeping similar learning performance. Interestingly, a ResNet can be understood as an implementation of a numerical time scheme solving a ODE/PDE (Ruthotto and Haber, 2019; Rousseau et al., 2019). Applications to learning PDEs from data have also been introduced *e.g.* PDE-Net (Long et al., 2017, 2018). These previous works emphasize the connection between the underlying physics and the NN architectures.

Designing or learning a NN representation for a given physical process remains a difficult issue. If the learning fails, it may be unclear to know how to improve the architecture of the neural network. Besides, it seems irrelevant to run computationally-



expensive numerical experiments on large-scale dataset to learn well-represented processes. The advection in fluid dynamics may be a typical example of such processes, which do not require complex non-linear data-driven representations. Overall, one would expect to accelerate and make more robust the learning process by combining, within the same NN architecture, the known physical equations with the unknown physics.

From the geoscience point of view, a key question is to bridge physical representations and neural network ones so that we can decompose both known and unknown equations according to the elementary computational units made available by state-of-the-art frameworks (e.g., keras, tensorflow). In other words, we aim to translate physical equations into the computational vocabulary available to neural networks. *PDE-NetGen* addresses this issue for PDE representations, for which we regard convolutional layers as being similar to the stencil approach, which results from a finite difference implementation of PDEs. *PDE-NetGen* relies on two main components: (i) a computer algebra system, here Sympy (Meurer et al., 2017), used to handle the physical equations and discretize the associated spatial derivatives, (ii) a Keras network generator which automatically translate PDEs into neural network layers from these discretized forms. Note that code generator based on symbolic computation receives new interests to facilitate the design of numerical experiments see e.g. Louboutin et al. (2019). As an illustration, we consider in this paper the application of *PDE-NetGen* to the identification of closure terms.

The paper is organized as follows. In the next section, we detail the proposed neural network generator, with an illustration of the workflow on a diffusion equation. In section 3, we present the numerical integration of the neural network implementation of the diffusion equation then an application to the data-driven identification of the closure of Burgers equation. Conclusion and perspective are given in section 4

2 Neural Network Generation from symbolic PDEs

Introducing physics in the design of neural network topology is challenging since physical processes can rely on very different partial derivative equations, e.g. eigenvalue problems for waves or constrained evolution equations in fluid dynamics under isovolumetric assumption. The neural network code generator presented here focuses on physical processes given as evolution equations which writes

$$\partial_t u = F(u, \partial^\alpha u), \tag{1}$$

where u denotes either a scalar field or multivariate fields, $\partial^\alpha u$ denotes partial derivatives with respect to spatial coordinates, and F is the generator of the dynamics. At first glance, this situation excludes diagnostic equation as encountered in geophysics, like balance equations: each equation has to be the evolution equation of a prognostic variable. *PDE-NetGen* incorporates a way to solve diagnostic equation, this will be shown in the example detailed in Section 3.2.

We first explain how the derivatives are embedded into NN layers, then we detail the workflow of *PDE-NetGen* for a simple example.



2.1 Introducing physical knowledge in the design of a NN topology

Since the NN generator is designed for evolution equations, the core of the generator is the automatic translation of partial derivatives with respect to spatial coordinates into layers. The correspondence between the finite-difference discretization and the convolutional layer give a practical way to translate a PDE into a NN (Cai et al., 2012; Dong et al., 2017; Long et al., 2017).

For instance, the finite difference of a second order partial derivative $\partial_x^2 u$, for $u(t, x)$ a one dimensional function, is given by

$$\partial_x^2 u(t, x) \approx \frac{u(t, x + \delta x) + u(t, x - \delta x) - 2u(t, x)}{\delta x^2}, \quad (2)$$

where δx stands for the discretization space step. This makes appear a kernel stencil $k = [1/\delta x^2, -2/\delta x^2, 1/\delta x^2]$ that can be used in a 1D convolution layer with a linear activation function and without bias. A similar routine applies for 2D and 3D geometries. *PDE-NetGen* relies on the computer algebra system *sympy* (Meurer et al., 2017) to compute the stencil as well as to handle symbolic expressions. Alternatives using automatic differentiation can be considered as introduced by Raissi (2018) who used TensorFlow for the computation of derivative.

Then, the time integration can be implemented either by a solver or by a ResNet architecture of a given time scheme *e.g.* an Euler scheme or a fourth order Runge-Kutta (RK4) scheme (Fablet et al., 2017).

These two components, namely the translation of partial derivatives into NN layers and a ResNet implementation of the time integration, are the building blocks of the proposed NN topology generator as exemplified in the next Section.

2.2 Workflow of the NN representation generator

We now present the workflow for the NN generator given a symbolic PDE using the heterogeneous 2D diffusion equation as a testbed:

$$\partial_t u = \nabla \cdot (\kappa \nabla u), \quad (3)$$

where $\kappa(x, y)$ is a field of 2×2 tensors ((x, y) are the spatial coordinates) and whose python implementation is detailed in Fig. 1.

Starting from a list of coupled evolution equations given as a PDE, a first preprocessing of the system determines the prognostic functions, the constant functions, the exogenous functions and the constants. The exogenous functions are the functions which depends on time and space, but whose evolution is not described by the system of evolution equations. For instance, a forcing term in a dynamics is an exogenous function.

For the diffusion equation Eq. (3), the dynamics is represented in *sympy* using *Function*, *Symbol* and *Derivative* classes. The dynamics is defined as an equation using the *Eq* class of *PDE-NetGen*, which inherits from the *Eq* class of *sympy* with additional facilities (see the implementation in Fig. 1 for additional details).

The core of the NN generator is given by the *NNModelBuilder* class. This class first preprocesses the system of evolution equations and translates the system into a python NN model.



```
from sympy import Function, symbols, Derivative
from pdenetgen.symbolic import Eq, NNModelBuilder

# Defines the diffusion equation using sympy
t, x, y = symbols('t x y')
u = Function('u')(t,x,y)
k11 = Function('\kappa_{11}')(x,y)
k12 = Function('\kappa_{12}')(x,y)
k22 = Function('\kappa_{22}')(x,y)

diffusion_in_2D = Eq(Derivative(u,t),
    Derivative(k11*Derivative(u,x)+
        k12*Derivative(u,y) ,x)+
    Derivative(k12*Derivative(u,x)+
        k22*Derivative(u,y) ,y)).doit()

# Defines the neural network code generator
diffusion_nn_builder = NNModelBuilder(diffusion_2D,
    class_name="NNDiffusion2DHeterogeneous")

# Renders the neural network code
exec(diffusion_nn_builder.code)

# Creates a 2D Diffusion model
diffusion_model = NNDiffusion2DHeterogeneous()
```

Figure 1. Neural Network generator for a heterogeneous 2D diffusion equation

The preprocessing of the diffusion equation Eq. (3) presents a single prognostic function, u , and three constant functions κ_{11} , κ_{12} and κ_{22} . There is no exogenous function for this example. During the preprocessing, the coordinate system of each function is diagnosed such that we may determine the dimension of the problem. For the diffusion equation Eq. (3), since the function $u(t, x, y)$ is a function of (x, y) the geometry is two-dimensional. In the current version of *PDE-NetGen*, only periodic boundaries are considered. The specific *DerivativeFactory* class ensures the periodic extension of the domain, then the computation of the derivative by using CNN and finally the crop of the extended domain to return to the initial domain. Other boundaries could also be implemented and might be investigated in future developments.

All partial derivatives with respect to spatial coordinates are detected and then replaced by an intermediate variable in the system of evolution equations. The resulting system is assumed to be algebraic, which means that it only contains addition, subtraction, multiplication and exponentiation (with at most a real). For each evolution equation, the abstract syntax tree is translated into a sequence of layers which can be automatically converted into NN layers in a given NN framework. For the current version of *PDE-NetGen*, we consider *Keras* (Chollet, 2018). An example of the implementation in *Keras* is shown in Fig. 2: a first part of the code is used to compute all the derivatives using Conv layers of *Keras*, then *Keras* layers are used to implement the algebraic equation which represents the trend $\partial_t u$ of the diffusion equation Eq. (3).

At the end, a python code is rendered from templates by using the *jinja2* package. The reason why templates are used is to facilitate the saving of the code in python modules and the modification of the code by the experimenter. Runtime computation of the class could be considered, but this is not implemented in the current version of *PDE-NetGen*. For the diffusion equation



```
# Example of computation of a derivative
kernel_Du_x_o1 = np.asarray([[0.0, -1/(2*self.dx[self.coordinates.index('x')]), 0.0],
                             [0.0, 0.0, 0.0],
                             [0.0, 1/(2*self.dx[self.coordinates.index('x')]), 0.0]]).reshape((3, 3)+(1,1))
Du_x_o1 = DerivativeFactory((3, 3), kernel=kernel_Du_x_o1, name='Du_x_o1')(u)

# Computation of trend_u
mul_1 = keras.layers.multiply([Dkappa_11_x_o1, Du_x_o1], name='MulLayer_1')
mul_2 = keras.layers.multiply([Dkappa_12_x_o1, Du_y_o1], name='MulLayer_2')
mul_3 = keras.layers.multiply([Dkappa_12_y_o1, Du_x_o1], name='MulLayer_3')
mul_4 = keras.layers.multiply([Dkappa_22_y_o1, Du_y_o1], name='MulLayer_4')
mul_5 = keras.layers.multiply([Du_x_o2, kappa_11], name='MulLayer_5')
mul_6 = keras.layers.multiply([Du_y_o2, kappa_22], name='MulLayer_6')
mul_7 = keras.layers.multiply([Du_x_o1_y_o1, kappa_12], name='MulLayer_7')
sc_mul_1 = keras.layers.Lambda(Lambda(x: 2.0*x, name='ScalarMulLayer_1')(mul_7))
trend_u = keras.layers.add([mul_1, mul_2, mul_3, mul_4, mul_5, mul_6, sc_mul_1], name='AddLayer_1')
```

Figure 2. Part of the python code of the *NNDiffusion2DHeterogeneous* class which implements the diffusion equation Eq. (3) as a neural-network by using Keras (only one derivative is explicitly given, for the sake of simplicity)

Eq. (3), when run, the code rendered from the *NNModelBuilder* class creates the *NNDiffusion2DHeterogeneous* class. Following the class diagram Fig. 3, the *NNDiffusion2DHeterogeneous* class inherits from a *Model* class which implements the time evolution of an evolution dynamics by incorporating a time-scheme. Here several time-schemes are implemented, namely an explicit Euler scheme, a second and a fourth order Runge-Kutta scheme.

105 3 Applications of PDE-NetGen

Two applications are now considered. First we validate the NN generator on a known physical problem: the diffusion equation Eq. (3) detailed in the previous section. Then, we tackle a situation where a part of the physics remains unknown, showing the benefit of merging the known physics in the learning of the unknown processes.

3.1 Application to the diffusion equation

110 In the python implementation Fig. 1, *diffusion_model* is an instance of the *NNDiffusion2DHeterogeneous* class, which numerically solves the diffusion equation Eq. (3) over a 2D domain, defined by default as the periodic domain $[0, 1) \times [0, 1)$ discretized by 100 points along each directions, so that $dx = dy = 1.0/100$.

The time integration of the diffusion equation is shown in Fig. 4. For this numerical experiment, the heterogeneous tensor field of diffusion tensors $\kappa(x, y)$ is set as rotations of the diagonal tensor $(l_x^2/\tau, l_y^2/\tau)$ defined from the length-scales $l_x = 10 dx$,
 115 $l_y = 5 dy$ and the time-scale $\tau = 1.0$, and with the rotation angles $\theta(x, y) = \frac{\pi}{3} \cos(k_x x + k_y y)$ where $(k_x, k_y) = 2\pi(2, 3)$. The time step for the simulation is $dt = \tau \text{Min}(dx^2/l_x^2, dy^2/l_y^2)/6$. The numerical integration is computed by using a fourth-order Runge-Kutta scheme. The initial condition of the simulation is given by a Dirac Fig. 4 (a). In order to validate the solution

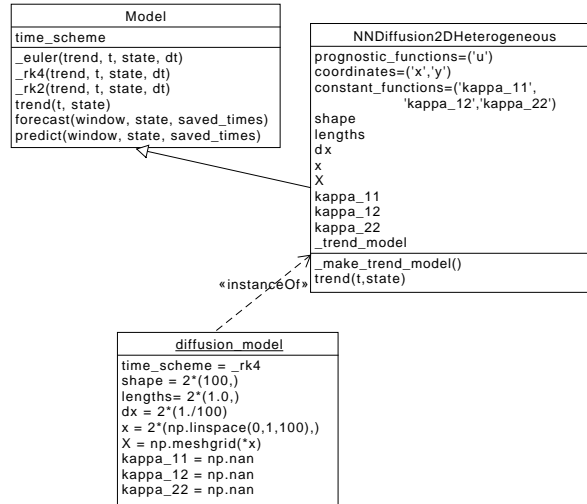


Figure 3. UML class diagram showing the interaction between the *Model* and the *NNDiffusion2DHeterogeneous* classes, and the resulting instance *diffusion_model* corresponding to the numerical computation of the diffusion equation Eq. (3).

obtained from the generated neural network, we compare the integration with the finite difference discretization of Eq. (3):

$$\begin{aligned}
 120 \quad \frac{\partial}{\partial t} u(t, x, y) = & -\frac{2\kappa_{22}(x, y)u(t, x, y)}{dy^2} + \frac{\kappa_{22}(x, y)u(t, x, -dy + y)}{dy^2} + \\
 & \frac{\kappa_{22}(x, y)u(t, x, dy + y)}{dy^2} + \frac{\kappa_{22}(x, -dy + y)u(t, x, -dy + y)}{4dy^2} - \\
 & \frac{\kappa_{22}(x, -dy + y)u(t, x, dy + y)}{4dy^2} - \frac{\kappa_{22}(x, dy + y)u(t, x, -dy + y)}{4dy^2} + \\
 & \frac{\kappa_{22}(x, dy + y)u(t, x, dy + y)}{4dy^2} + \frac{\kappa_{12}(x, y)u(t, -dx + x, -dy + y)}{2dxdy} - \\
 & \frac{\kappa_{12}(x, y)u(t, -dx + x, dy + y)}{2dxdy} - \frac{\kappa_{12}(x, y)u(t, dx + x, -dy + y)}{2dxdy} + \\
 125 \quad & \frac{\kappa_{12}(x, y)u(t, dx + x, dy + y)}{2dxdy} + \frac{\kappa_{12}(x, -dy + y)u(t, -dx + x, y)}{4dxdy} - \\
 & \frac{\kappa_{12}(x, -dy + y)u(t, dx + x, y)}{4dxdy} - \frac{\kappa_{12}(x, dy + y)u(t, -dx + x, y)}{4dxdy} + \\
 & \frac{\kappa_{12}(x, dy + y)u(t, dx + x, y)}{4dxdy} + \frac{\kappa_{12}(-dx + x, y)u(t, x, -dy + y)}{4dxdy} - \\
 & \frac{\kappa_{12}(-dx + x, y)u(t, x, dy + y)}{4dxdy} - \frac{\kappa_{12}(dx + x, y)u(t, x, -dy + y)}{4dxdy} + \\
 & \frac{\kappa_{12}(dx + x, y)u(t, x, dy + y)}{4dxdy} - \frac{2\kappa_{11}(x, y)u(t, x, y)}{dx^2} + \\
 130 \quad & \frac{\kappa_{11}(x, y)u(t, -dx + x, y)}{dx^2} + \frac{\kappa_{11}(x, y)u(t, dx + x, y)}{dx^2} + \\
 & \frac{\kappa_{11}(-dx + x, y)u(t, -dx + x, y)}{4dx^2} - \frac{\kappa_{11}(-dx + x, y)u(t, dx + x, y)}{4dx^2} - \\
 & \frac{\kappa_{11}(dx + x, y)u(t, -dx + x, y)}{4dx^2} + \frac{\kappa_{11}(dx + x, y)u(t, dx + x, y)}{4dx^2} \quad (4)
 \end{aligned}$$

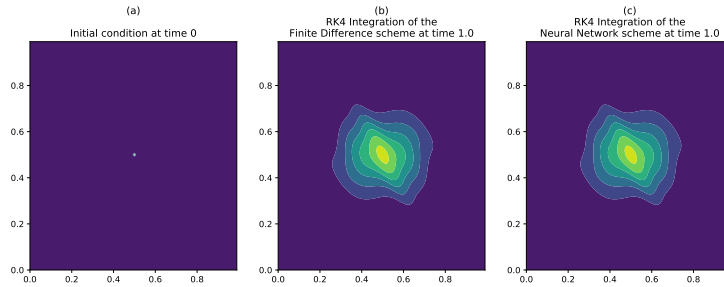


Figure 4. Starting from a Dirac (panel a), the diffusion equation Eq. (3) is integrated from 0 to 1 by using a fourth-order Runge-Kutta time scheme. The results obtained from the time integration of the finite difference implementation Eq. (4) (panel b) and of the generated NN representation (panel c) are similar.

which is shown in Fig. 4 (b). The heterogeneity of the diffusion tensors makes appear an anisotropic diffusion of the Dirac, which is perfectly reproduced by the result obtained from the integration of the generated neural network, shown in Fig. 4 (c).
135 At a quantitative level, the l^2 distance between the both solutions is 10^{-5} . This validates the ability of the NN generator *PDE-NetGen* to compute the dynamics of a given physical evolution equation.

The next section illustrates the situation where only a part of the dynamics is known, while the remaining physics is learned from the data.

3.2 Application to the data-driven identification of stochastic representations

140 As an illustration of the *PDE-NetGen* package, we consider a problem encountered in uncertainty prediction: the parametric Kalman filter (PKF) (Pannekoucke et al., 2016, 2018). For a detailed presentation and discussion of uncertainty prediction issues in geophysical dynamics, we may refer the reader to Le Maître and Knio (2010). Here, we briefly introduce basic elements for the self-consistency of the example.

The idea of the PKF is to mimic the dynamics of the covariance-error matrices all along the analysis and the forecast cycle
145 of the data assimilation in a Kalman setting (Kalman filter equations for the uncertainty). It relies on the approximation of the true covariance matrices by some parametric covariance model. When considering a covariance model based on a diffusion equation, the parameters are the variance V and the local diffusion tensor ν . Therefore, the dynamics of the covariance-error matrices along the data assimilation cycles is deduced from the dynamics of the variance and of the diffusion tensors. In place of the full covariance evolution this dramatically reduces the dynamics to the one of few parameters.

150 For the non-linear advection-diffusion equation, known as the Burgers equation,

$$\partial_t u + u \partial_x u = \kappa \partial_x^2 u, \quad (5)$$



the dynamics of the variance V_u and the diffusion tensor $\nu_u = [\nu_{u,xx}]$ (which is featured by a single field $\nu_{u,xx}$), writes (Pannekoucke et al., 2018)

$$\left\{ \begin{array}{l} \frac{\partial}{\partial t} u = \kappa \frac{\partial^2}{\partial x^2} u - u \frac{\partial}{\partial x} u - \frac{\partial}{\partial x} V_u \\ \frac{\partial}{\partial t} V_u = -\frac{\kappa V_u}{\nu_{u,xx}} + \kappa \frac{\partial^2}{\partial x^2} V_u - \frac{\kappa \left(\frac{\partial}{\partial x} V_u \right)^2}{2 V_u} \\ \quad - u \frac{\partial}{\partial x} V_u - 2 V_u \frac{\partial}{\partial x} u \\ \frac{\partial}{\partial t} \nu_{u,xx} = 4 \kappa \nu_{u,xx}^2 \mathbb{E} \left[\varepsilon_u \frac{\partial^4}{\partial x^4} \varepsilon_u \right] \\ \quad - 3 \kappa \frac{\partial^2}{\partial x^2} \nu_{u,xx} - \kappa + \frac{6 \kappa \left(\frac{\partial}{\partial x} \nu_{u,xx} \right)^2}{\nu_{u,xx}} \\ \quad - \frac{2 \kappa \nu_{u,xx} \frac{\partial^2}{\partial x^2} V_u}{V_u} + \frac{\kappa \frac{\partial}{\partial x} V_u \frac{\partial}{\partial x} \nu_{u,xx}}{V_u} + \\ \quad \frac{2 \kappa \nu_{u,xx} \left(\frac{\partial}{\partial x} V_u \right)^2}{V_u^2} - u \frac{\partial}{\partial x} \nu_{u,xx} + \\ \quad 2 \nu_{u,xx} \frac{\partial}{\partial x} u \end{array} \right. \quad (6)$$

155 where $\mathbb{E}[\cdot]$ denotes the expectation operator. For the sake of simplicity, in this system of PDEs, u denotes the expectation of the random field and not the random field itself as in (Eq. (5)).

In this system of PDEs, the term $\mathbb{E} \left[\varepsilon_u \frac{\partial^4}{\partial x^4} \varepsilon_u \right]$ can not be determined from the known quantities u , V_u and $\nu_{u,xx}$. This makes appear a closure problem, *i.e.* determining the unknown term as a function of the known quantities. A naive assumption would be to consider a zero closure (closure(t, x) = 0). However, while the tangent-linear evolution of the perturbations along the Burgers dynamics is stable, the dynamics of the diffusion coefficient $\nu_{u,xx}$ would lead to unstable dynamics as the coefficient of the second order term $-3\kappa \frac{\partial^2}{\partial x^2} \nu_{u,xx}$ is negative. This stresses further the importance of the unknown term to successfully predict the uncertainty.

165 Within a data-driven framework, one would typically explore a direct identification of the dynamics of diffusion coefficient $\nu_{u,xx}$. Here, we exploit *PDE-NetGen* to fully exploit the known physics and focus on the data-driven identification of the unknown term $\mathbb{E} \left[\varepsilon_u \frac{\partial^4}{\partial x^4} \varepsilon_u \right]$ in the system of equations Eq. (6). It comes to replace term $\mathbb{E} \left[\varepsilon_u \frac{\partial^4}{\partial x^4} \varepsilon_u \right]$ in Eq. (6) by an exogenous function *closure*(t, x) and then to follow the workflow detailed in Section 2.2.

The unknown closure function is represented by a neural network (a Keras model) which implements the expansion

$$\text{closure}(t, x) \sim a \frac{\frac{\partial^2}{\partial x^2} \nu_{u,xx}(t, x)}{\nu_{u,xx}^2(t, x)} + b \frac{1}{\nu_{u,xx}^2(t, x)} + c \frac{\left(\frac{\partial}{\partial x} \nu_{u,xx}(t, x) \right)^2}{\nu_{u,xx}^3(t, x)} \quad (7)$$

170 where (a, b, c) are unknown and where the partial derivatives are computed from convolution layers, as described in Section 2. This expression is similar to a dictionary of possible terms as in Rudy et al. (2017) and it is inspired from an arbitrary theoretically-designed closure for this problem, where (a, b, c) = $(1, \frac{3}{4}, -2)$ (Pannekoucke et al., 2018). In the NN implementation of the exogenous function modeled as Eq. (7), each of the unknown coefficients (a, b, c) are implemented as a 1D convolutional layer, with a linear activation function and without bias. Note that the estimated parameters (a, b, c) could be different from the one of the theoretical closure: while the theoretical closure can give some clues for the design of the unknown term, this closure is not the truth which is unknown.

For the numerical experiment, the Burgers equation is solved on a one-dimensional periodic domain of length 1, discretized in 241 points. The time step is $dt = 0.002$, and the dynamics is computed over 500 time steps so to integrate from $t = 0$ to



```
def make_time_scheme(dt, trend):  
    """ Keras implementation for a RK4 """  
    import keras  
  
    state = keras.layers.Input(shape = trend.input_shape[1:])  
  
    # k1  
    k1 = trend(state)  
    # k2  
    _tmp_1 = keras.layers.Lambda(Lambda(x : 0.5*dt*x))(k1)  
    input_k2 = keras.layers.add([state, _tmp_1])  
    k2 = trend(input_k2)  
    # k3  
    _tmp_2 = keras.layers.Lambda(Lambda(x : 0.5*dt*x))(k2)  
    input_k3 = keras.layers.add([state, _tmp_2])  
    k3 = trend(input_k3)  
    # k4  
    _tmp_3 = keras.layers.Lambda(Lambda(x : dt*x))(k3)  
    input_k4 = keras.layers.add([state, _tmp_3])  
    k4 = trend(input_k4)  
  
    # output  
    # k2+k3  
    add_k2_k3 = keras.layers.add([k2, k3])  
    add_k2_k3_mul2 = keras.layers.Lambda(Lambda(x:2.*x))(add_k2_k3)  
    # Add k1, k4  
    _sum = keras.layers.add([k1, add_k2_k3_mul2, k4])  
    # *dt  
    _sc_mul = keras.layers.Lambda(Lambda(x:dt/6.*x))(_sum)  
    output = keras.layers.add([state, _sc_mul])  
  
    time_scheme = keras.models.Model(inputs=[state],  
                                     outputs=[output])  
  
    return time_scheme
```

Figure 5. Example of a Keras implementation for a RK4 time-scheme: given time-step dt and a Keras model $trend$ of the dynamics, the function $make_time_scheme$ return a Kera model implementing a RK4.

180 $t = 1.0$. The coefficient of the physical diffusion is set to $\kappa = 0.0025$. The numerical setting considered for the learning is the tangent-linear regime described in Pannekoucke et al. (2018) where the initial uncertainty is small and whose results are shown in their Fig. 4(a), Fig. 5(a) and Fig. 6(a).

To train the parameters (a, b, c) in Eq. (7), we build a training dataset from an ensemble prediction method where each member is a numerical solution of the Burgers equation. The numerical code for the Burgers equation derives from *PDE-NetGen* applied on the symbolic dynamics Eq. (5). Using this numerical code, we generate a training dataset composed of 400 ensemble simulations of 501 time steps, where each each ensemble contains 400 members. For each ensemble forecast, we estimate the mean, variance V_u and diffusion tensor ν_u . Here, we focus on the development of the front where we expect the unknown term to be of key importance and keep for training purposes the last 100 time-steps of each ensemble forecast. For the training only, the RK4 time-scheme is computed as the ResNet implementation given in Fig. 5, so to provide the end-to-end NN implementation of the dynamics.

190 The resulting dataset involves 40000 samples. To train the learnable parameters (a, b, c) , we minimize the one-step ahead prediction loss for the diffusion tensor ν_u . We use ADAM optimizer (Kingma and Ba, 2014) and a batch size of 32. Using an initial learning rate of 0.1, the training converges within 3 epochs with a geometrical decay of the learning rate by a factor of 1/10 after each epoch. The coefficients resulting from the training over 10 runs are $(a, b, c) = (0.93, 0.75, -1.80) \pm (5.1 \cdot 10^{-5}, 3.6 \cdot 10^{-4}, 2.7 \cdot 10^{-4})$.

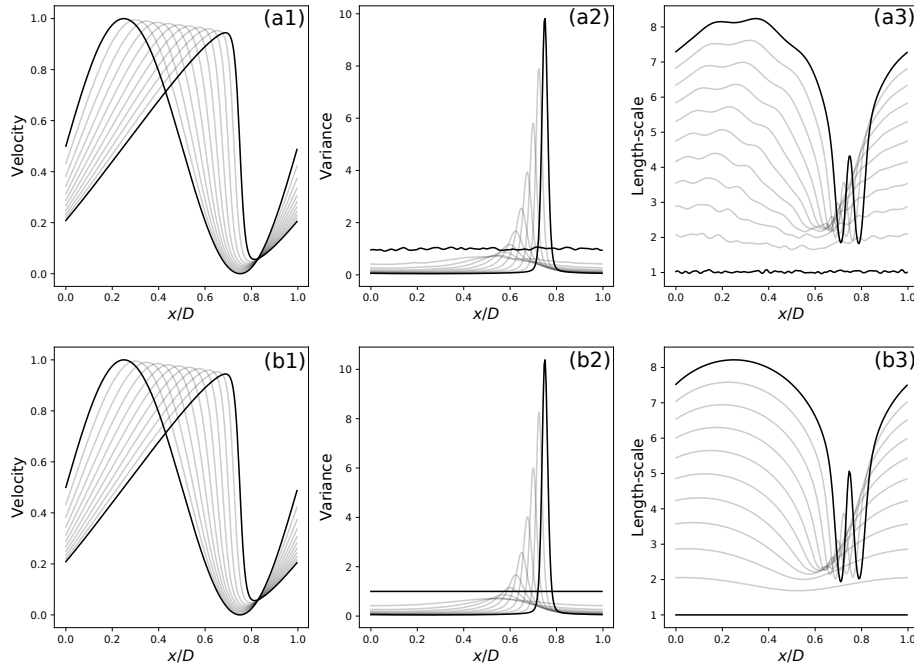


Figure 6. Uncertainty estimated from a large ensemble of 1000 members (a) with the expectation $\mathbb{E}[u]$ (a1), variance V_u (a2) and the length-scale (defined from the diffusion coefficient by $\sqrt{0.5\nu_{u,xx}}$) (a3); and the uncertainty predicted from the PKF evolution equations closed from the data (b), where the same statistics are shown in (b1), (b2) and (b3). The fields are represented only for time $t = 0, 0.2, 0.4, 0.6, 0.8, 1$

Figure 6 compares the estimation from a large ensemble of 1000 members (top panels) with the results of the trained closed
 195 PKF dynamics (bottom panels). Both the ensemble and PKF means (a1) and (b1) clearly show a front which emerges from
 the smooth initial condition and located near $x = 0.75$ at time 1.. The variance fields (a2) and (b2) illustrate the vanishing
 of the variance due to the physical diffusion (the κ term in Eq. (5)) and the emergence of a pic of uncertainty which is
 related to the uncertainty of the front position. Instead of the diffusion $\nu_{u,xx}$, panels (a3) and (b3) show the evolution of the
 correlation length-scale defined as $\sqrt{0.5\nu_{u,xx}}$, which has the physical dimension of a length. Both panels show the increase of
 200 the length-scale due to the physical diffusion, except in the vicinity of the front where an oscillation occurs, which is related
 to the inflexion point of the front. While the magnitude of the oscillation predicted by the PKF (b3) is slightly larger than the
 estimation from the large ensemble reference (a3), the pattern is well predicted by the PKF. Besides, the parametric form of the
 PKF does not involve local variabilities due to the finite size of the ensemble, which may be observed in panel (a3). Overall,
 these experiments support the relevance of the closure Eq. (7) learned from the data to capture the uncertainty associated with
 205 Burgers' dynamics.

3.3 Discussion on the choice of a closure

In the Burgers' dynamics, an a priori knowledge was introduced to propose a NN implementing the closure Eq. (7).



In the general case, the choice of the terms to be introduced in the closure may be guided by known physical properties that need to be verified by the system. For example, conservation or symmetries properties that leave the system invariant can guide in proposing possible terms. For the Burgers' dynamics, $\nu_{u,xx}$ has the dimension of a length squared, $[L^2]$, and $\mathbb{E} \left[\varepsilon_u \frac{\partial^4}{\partial x^4} \varepsilon_u \right]$ is of dimension $[L^{-4}]$. Thus, the terms considered in Eq. (7) are among the simplest ones which fulfill the expected dimensionality of $[L^{-4}]$. Symbolic computation may here help the design of such physical parameterizations in more general cases.

When no priors are available, one may consider modeling the closure using state-of-the-art deep neural network architectures which have shown impressive prediction performance, e.g. CNNs, ResNets (Zagoruyko and Komodakis, 2016; Raissi, 2018).

4 Conclusions

We have introduced a neural network generator *PDE-NetGen*, which provides new means to bridge physical priors given as symbolic PDEs and learning-based NN frameworks. This package derives and implements a finite difference version of a system of evolution equations, where the derivative operators are replaced by appropriate convolutional layers including the boundary conditions. The package has been developed in python using the symbolic mathematics library *sympy* and *keras*.

We have illustrated the usefulness of *PDE-NetGen* through two applications: a neural-network implementation of a 2D heterogeneous diffusion equation and the uncertainty prediction in the Burgers equation. The later involves unknown closure terms, which are learned from data using the proposed neural-network framework. Both illustrations show the potential of such an approach, which could be useful for improving the training in complex application by taking into account the physics of the problem.

This work opens new avenues to make the most of existing physical knowledge and of recent advances in data-driven settings, and more particularly neural networks, for geophysical applications. This includes a wide range of applications, where such physically-consistent neural network frameworks could either lead to the reduction of the computational cost (e.g., GPU implementation embedded in deep learning frameworks) or provide new numerical tools to derive key operators (e.g., adjoint operator using automatic differentiation). Besides, these neural network representations also offer new means to complement known physics with the data-driven calibration of unknown terms. This is regarded as key to advance the state-of-the-art for the simulation, forecasting and reconstruction of geophysical dynamics through model-data-coupled frameworks.

Code availability. Code of *PDE-NetGen* is available on github in version 1.0: <https://github.com/opannekoucke/pdenetgen>

Author contributions. OP and RF designed the study, conducted the analysis, and wrote the manuscript. OP developed the code.



235 *Competing interests.* The authors declare that they have no conflict of interest.

Acknowledgements. The UML class diagram has been generated from UMLlet Auer et al. (2003). This work was supported by the French national program LEFE/INSU (Étude du filtre de KAlman PAramétrique, KAPA). RF has been partially supported by Labex Cominlabs

(grant SEACS), CNES (grant OSTST-MANATEE) and ANR through programs EUR Isblue, Melody and OceaniX.





References

- 240 Auer, M., Tschurtschenthaler, T., and Biffl, S.: A Flyweight UML Modelling Tool for Software Development in Heterogeneous Environments, in: Proceedings of the 29th Conference on EUROMICRO, EUROMICRO '03, pp. 267–, IEEE Computer Society, Washington, DC, USA, <http://dl.acm.org/citation.cfm?id=942796.943259>, 2003.
- Cai, J.-F., Dong, B., Osher, S., and Shen, Z.: Image restoration: Total variation, wavelet frames, and beyond, *Journal of the American Mathematical Society*, 25, 1033–1089, <https://doi.org/10.1090/s0894-0347-2012-00740-1>, 2012.
- 245 Chollet, F.: *Deep Learning with Python*, Manning Publications, 2018.
- Dong, B., Jiang, Q., and Shen, Z.: Image Restoration: Wavelet Frame Shrinkage, Nonlinear Evolution PDEs, and Beyond, *Multiscale Modeling & Simulation*, 15, 606–660, <https://doi.org/10.1137/15m1037457>, 2017.
- Fablet, R., Ouala, S., and Herzet, C.: Bilinear residual Neural Network for the identification and forecasting of dynamical systems, *ArXiv*, <http://arxiv.org/abs/1712.07003v1>, 2017.
- 250 He, K., Zhang, X., Ren, S., and Sun, J.: Deep Residual Learning for Image Recognition, in: 2016 IEEE Conference on Computer Vision and Pattern Recognition (CVPR), IEEE, <https://doi.org/10.1109/cvpr.2016.90>, 2016.
- Kingma, D. P. and Ba, J.: Adam: A Method for Stochastic Optimization, *ArXiv*, 2014.
- Le Maître, O. P. and Knio, O. M.: *Spectral Methods for Uncertainty Quantification*, Springer Netherlands, <https://doi.org/10.1007/978-90-481-3520-2>, 2010.
- 255 Long, Z., Lu, Y., Ma, X., and Dong, B.: PDE-Net: Learning PDEs from Data, *ArXiv*, <https://arxiv.org/abs/1710.09668>, 2017.
- Long, Z., Lu, Y., and Dong, B.: PDE-Net 2.0: Learning PDEs from Data with A Numeric-Symbolic Hybrid Deep Network, *ArXiv*, <http://arxiv.org/pdf/1812.04426v2>, 2018.
- Louboutin, M., Lange, M., Luporini, F., Kukreja, N., Witte, P. A., Herrmann, F. J., Velesko, P., and Gorman, G. J.: Devito (v3.1.0): an embedded domain-specific language for finite differences and geophysical exploration, *Geoscientific Model Development*, 12, 1165–
260 1187, <https://doi.org/10.5194/gmd-12-1165-2019>, 2019.
- Mallat, S.: Understanding deep convolutional networks, *Philosophical Transactions of the Royal Society A: Mathematical, Physical and Engineering Sciences*, 374, 20150203, <https://doi.org/10.1098/rsta.2015.0203>, 2016.
- Meurer, A., Smith, C. P., Paprocki, M., Čertík, O., Kirpichev, S. B., Rocklin, M., Kumar, A., Ivanov, S., Moore, J. K., Singh, S., Rathnayake, T., Vig, S., Granger, B. E., Muller, R. P., Bonazzi, F., Gupta, H., Vats, S., Johansson, F., Pedregosa, F., Curry, M. J., Terrel, A. R., Roučka,
265 Š., Saboo, A., Fernando, I., Kulal, S., Cimrman, R., and Scopatz, A.: SymPy: symbolic computing in Python, *PeerJ Computer Science*, 3, e103, <https://doi.org/10.7717/peerj-cs.103>, 2017.
- Pannekoucke, O., Ricci, S., Barthelemy, S., Menard, R., and Thual, O.: Parametric Kalman Filter for chemical transport model, *Tellus*, 68, 31547, <https://doi.org/10.3402/tellusa.v68.31547>, 2016.
- Pannekoucke, O., Bocquet, M., and Ménard, R.: Parametric covariance dynamics for the nonlinear diffusive Burgers' equation, *Non-linear Processes in Geophysics*, 2018, 1–21, <https://doi.org/10.5194/npg-2018-10>, <https://www.nonlin-processes-geophys-discuss.net/npg-2018-10/>, 2018.
- 270 Raissi, M.: Deep Hidden Physics Models: Deep Learning of Nonlinear Partial Differential Equations, *J. Mach. Learn. Res.*, 19, 932–955, 2018.
- Rousseau, F., Drumetz, L., and Fablet, R.: Residual Networks as Flows of Diffeomorphisms, *Journal of Mathematical Imaging and Vision*,
275 <https://doi.org/10.1007/s10851-019-00890-3>, 2019.



Rudy, S. H., Brunton, S. L., Proctor, J. L., and Kutz, J. N.: Data-driven discovery of partial differential equations, *Science Advances*, 3, e1602 614, <https://doi.org/10.1126/sciadv.1602614>, 2017.

Ruthotto, L. and Haber, E.: Deep Neural Networks Motivated by Partial Differential Equations, *Journal of Mathematical Imaging and Vision*, <https://doi.org/10.1007/s10851-019-00903-1>, 2019.

280 Zagoruyko, S. and Komodakis, N.: Wide Residual Networks, in: *BMVC*, 2016.